Article

Robust Data-Driven Design for Fault Diagnosis of Industrial Drives

Umair Rashid [1,*], **Muhammad Asim Abbasi** [1,*], **Abdul Qayyum Khan** [1], **Muhammad Irfan** [2], **Muhammad Abid** [1] and **Grzegorz Nowakowski** [3]

1   Electrical Engineering Department, Pakistan Institute of Engineering and Applied Sciences, Islamabad 44000, Pakistan
2   Electrical Engineering Department, College of Engineering, Najran University, Najran 61441, Saudi Arabia
3   Faculty of Electrical and Computer Engineering, Cracow University of Technology, Warszawska 24 Str., 31-155 Cracow, Poland
*   Correspondence: umair851@gmail.com (U.R.); engrasimabbasi@gmail.com (M.A.A.)

Abstract: Due to the presence of actuator disturbances and sensor noise, increased false alarm rate and decreased fault detection rate in fault diagnosis systems have become major concerns. Various performance indexes are proposed to deal with such problems with certain limitations. This paper proposes a robust performance-index based fault diagnosis methodology using input–output data. That data is used to construct robust parity space using the subspace identification method and proposed performance index. Generated residual shows enhanced sensitivity towards faults and robustness against unknown disturbances simultaneously. The threshold for residual is designed using the Gaussian likelihood ratio, and the wavelet transformation is used for post-processing. The proposed performance index is further used to develop a fault isolation procedure. To specify the location of the fault, a modified fault isolation scheme based on perfect unknown input decoupling is proposed that makes actuator and sensor residuals robust against disturbances and noise. The proposed detection and isolation scheme is implemented on the induction motor in the experimental setup. The results have shown the percentage fault detection of 98.88%, which is superior among recent research.

Keywords: fault detection; fault Isolation; data-driven; industrial drives; subspace identification

1. Introduction

The early and accurate detection of abnormal events is crucial for today's safety-critical systems with their continuously increasing complexity. Model based fault diagnosis has enjoyed considerable attention during the last three decades and provides a rich literature of techniques considering practical solutions for fault diagnosis [1–7]. High-fidelity modeling requirements for model based fault diagnosis make it difficult and sometimes infeasible to implement for the complex system. Noteworthy examples from these complicated systems are networked control systems, internet of things [8], and different chemical industry processes [9]. A sufficient amount of data is available for the majority of such systems. This data contain information about the system, disturbances and noise, fault, and so on. To deal with such systems, various data-driven methods are being used with effective implementation.

These methods are broadly classified into two classes [10]: (1) data-driven methodologies [11,12]; (2) model-data based hybrid approaches [13–15]. Among various pure data based methods, machine learning [16], deep learning [17,18], and multivariate techniques including principal component analysis [19–21] and partial least square methods [22–24] are widely used with promising results. A model-data based hybrid approach usually considers the development of FDI schemes that consists of an intersection between model based and data-driven techniques [13]. Subspace identification method (SIM) emerged as one of the major techniques in this domain for the last two decades [25–28]. The key concept behind the Subspace identification method (SIM) approach is to identify the parity

space for the construction of observer based fault detection and isolation (FDI) scheme [26] or parity based FDI residual generators [27] using input–output data. The effect of external factors such as noise and disturbances from recorded data are eliminated by introducing instrument variables. Finding orthogonal projection of an extended observability matrix enables constructing residuals based on a parity vector, which is made possible by using the singular value decomposition (SVD) on covariance matrices of recorded data [29]. Since the Subspace identification method (SIM) is developed to estimate the dynamic model of the underlying system, it is worth mentioning that it also solves the problem of dealing with stationary as well as dynamical systems, compared to multivariate analysis (MVA) techniques which are operated on stationary processes. Although several MVA techniques have been developed to deal with dynamic issues, these are not suitable for stationary processes [30].

Subspace identification has been applied to many practical systems including the Tennessee Eastman process [26,31], vehicle lateral dynamic system [27], coupled liquid tank system [32], wind turbine benchmark [33–35], and three phase induction motor [36,37]. Since induction motors play a vital role in the process industry for converting electrome-chanical energy and are the most widely used devices [38], our study would be directed toward implementing data-driven techniques on an induction motor. Due to the critical operation of induction motors in industries such as power generation, petroleum [39], aerospace [40], and the medical industry, it is required to monitor the reliability and run-ning conditions to avoid any disastrous failures. Now, operators have started using rapid fault detection along with the usually planned maintenance, which could reduce the failure rate, increase the plant uptime, and reduce operational and maintenance costs.

The induction motor and its drive system could be subjected to different types of faults. Some of them could be [41,42]:

1. Stator fault that includes short and open circuiting of the stator winding;
2. Rotor faults dealing with end-ring cracking in the case of squirrel cage motor and short or open circuiting of the rotor winding;
3. Power supply failure due to power electronics damage of the driving system;
4. Mechanical fault including bearing damage, eccentricity misalignment, and a bent shaft.

Since induction motors are considered symmetrical machines, any fault could modify their operational behavior by changing symmetrical properties.

Machine learning and model-based methodologies have also been applied to induction motor for fault detection and isolation purposes. Convolutional neural network (CNN) based fault diagnosis and classification was carried out by Maciej Skowron in [43]. Dur-ing the fault detection process, a neural network also acts as a classification system which also identifies degree of damage to the induction motor. Choosing a right structure of CNN for fault detection and isolation (FDI) system plays a vital role in methodology, as a minor change could lead to a huge increase in false alarm rate (FAR). Data based and model based techniques have their own advantages and disadvantages in different system states. Unknown faults can be detected and identified efficiently by model based methods while data based methodologies mostly analyse the input–output signal of the induction motor giving low weight to system dynamics [44]. Hybrid approaches, which are a combination of system model based FDI schemes and pure data based methodologies, have shown great ability to detect fault and analyse fault with unbalanced conditions [45].

Parity equation based methods provide less online computational complexity which leads to early detection of faults [46]. In our FDI scheme, parity space is identified using a subspace identification method which is further used for residual generation. For the subspace method, it is challenging to find an optimal parity vector that makes generated residuals more sensitive towards fault and less sensitive towards external factors (e.g., noise and disturbances) simultaneously. To face such challenges, various performance indexes are proposed [26,27,32,37] for the computation of optimal parity vector. In [27], a proposed index considers the sensitivity for actuator and sensor faults but does not consider the effect of unknown inputs. Similarly, Ref. [32] proposed a performance index that considers the

effect of actuator disturbance and actuator fault sensitivity in generated residual. Till then, enhancement of sensitivity towards sensor faults and sensor noise was discussed. However, Ref. [37] proposed a methodology to optimize the parity vector for sensor fault and noise at the expense of actuator fault and disturbance.

In this paper, we have developed the subspace-based data-driven fault diagnosis scheme for dynamical systems based on the proposed performance index, which makes the residual sensitive towards actuator and sensor faults simultaneously while suppressing the effect of unknown inputs such as actuator disturbances and sensor noise. Furthermore, to determine the location of the faulty component, an isolation algorithm based on perfect unknown input decoupling is proposed with an improved performance index for an optimized parity vector.

The rest of the paper is organized as follows: Section 2 includes dynamic consideration of induction motor used for online implementation. Section 3 states the fundamentals of the subspace identification method and mathematical derivations. Proposed fault detection and isolation algorithms are also stated in Sections 3 and 4, respectively. Section 5 is related to the post-processing of residuals, which include wavelet transformation and Gaussian Likelihood Ration test. Practical implementation of developed schemes is then implemented on an induction motor as described in Section 6. Section 7 concludes with a summary of the work.

2. Induction Motor Dynamics

The induction motor is operated by applying AC voltage to the stator, which produces the AC current in the rotor circuit. Since there is no electrical connection between the rotor and stator of the induction motor, it makes the motor almost maintenance-free and more efficient due to no power loss in the commutators. Squirrel cage induction motors are the most commonly used motor varying from a few to hundreds of horsepower. The rotor rotates when it is subjected to varying magnetic fields, and the speed of the rotor depends upon the frequency (f_e) of applied voltage and stator poles (p) of the motor as described in Equation (1):

$$n_{sync} = \frac{120 f_e}{p} \tag{1}$$

A mathematical model of the motor could be constructed by considering the equivalent model of a signal phase induction motor. The nominal parameters of induction motor under consideration are given in Table 1. A 5th order state-space model of the induction motor is constructed based on the stator-fixed frame reference:

$$\begin{cases} \dot{\eta}_1 = c_4 \eta_1 - P_n \eta_5 \eta_2 + c_5 \eta_3 \\ \dot{\eta}_2 = P_n \eta_5 \eta_1 + c_4 \eta_2 + c_5 \eta_4 \\ \dot{\eta}_3 = c_6 \eta_1 + c_7 \eta_5 \eta_2 - \gamma \eta_3 + c_8 u_1 \\ \dot{\eta}_4 = -c_7 \eta_5 \eta_1 + c_6 \eta_2 - \gamma \eta_4 + c_8 u_2 \\ \dot{\eta}_5 = c_1 \eta_1 \eta_4 + c_2 \eta_5 + c_3 \tau_L - c_1 \eta_2 \eta_3 \\ y = [\eta_3, \eta_4] \end{cases} \tag{2}$$

Here, the state vector is representing the d-q axis fluxes and current along with the speed of rotor, such that $\eta = [\eta_1 \ \eta_2 \ \eta_3 \ \eta_4 \ \eta_5]^T = [\phi_d \ \phi_q \ i_d \ i_q \ \omega]^T$. Since motor is being activated by the three phase voltage, the acting actuator input would be these supply voltages.

Constants used in the model (2) are defined as

$$c_1 = \frac{P_n L_{s,r}}{D_m L_{rot}}, \qquad c_2 = -\frac{R_m}{D_m}, \qquad c_3 = -\frac{1}{D_m}$$

$$c_4 = -\frac{1}{T_r}, \qquad c_5 = \frac{L_{s,r}}{T_r}, \qquad c_6 = \frac{L_{s,r}}{T_r \sigma L_{sat} L_{rot}}$$

$$c_7 = \frac{P_n L_{s,r}}{\sigma L_{sat} L_{rot}}, \qquad c_8 = \frac{1}{\sigma L_{sat}}$$

further,

$$\gamma = \frac{R_{sat}}{L_{sat}\sigma} + \frac{L_{s,r}^2}{\sigma L_{sat} L_{rot} T_{rot}}, \qquad \sigma = 1 - \frac{L_{s,r}^2}{L_{sat} L_{rot}}$$

$$T_r = \frac{L_{rot}}{R_{rot}}$$

Thus, the dynamic model for an induction motor (SE2672-3G) as shown in Figure 1 could be found using values given in Table 1. Besides nominal parameters, the nominal operating conditions of motor are stated in Table 2.
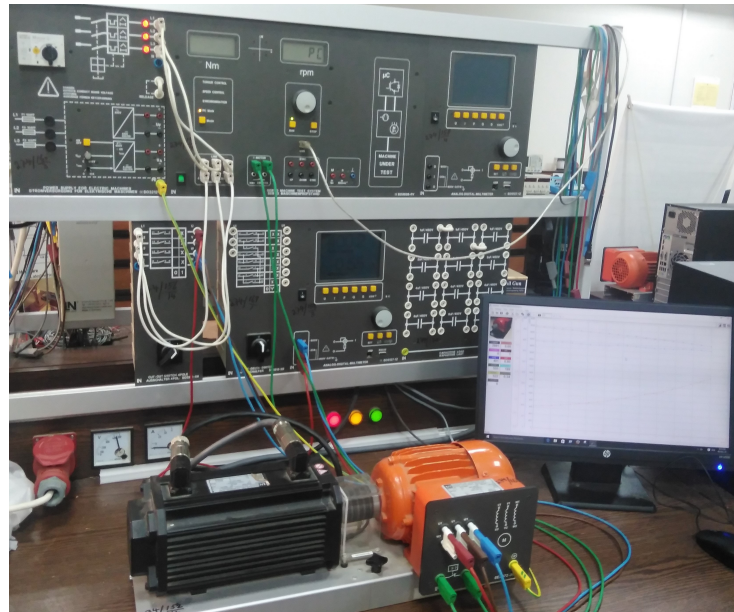

Figure 1. Experimental setup of Industrial drive (SE2672-3G).

Table 1. Induction Motor Nominal Parameters (SE2672-3G).

Name	Symbol	Value
Number of poles	P_n	2
Inductance of Rotor	L_{rot}	0.1164
Resistance of Rotor	R_{rot}	3.5735
Inductance of Stator	L_{sat}	0.1164
Resistance of Stator	R_{sat}	0.7941
Leakage factor	σ	0.092896
Mutual inductance	$L_{s,r}$	0.1109

Table 2. Nominal operating conditions (SE2672-3G).

Parameter	Value
Nominal Voltage Δ/Y	400/690 V
Nominal Current Δ/Y	1.0/0.6 A
Nominal Power	370 W
Power Factor	0.83
Frequency	50 Hz
Nominal Speed	2800 rpm

3. Fault Diagnosis Scheme

Parity vector-based residual generation is one of the famous fault diagnosis schemes used in both model-based and data-driven FDI systems [47]. The parity vector scheme allows us to use techniques developed in model-based FDI literature for data-driven systems.

In order to obtain the advantage of the availability of input–output data samples of the process and avoid complexity issues to obtain a system model, the subspace identification mechanism is focused on this work as expressed in Figure 2.
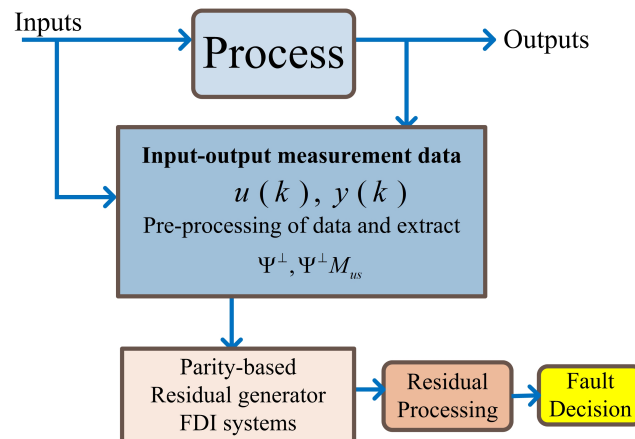
Figure 2. Subspace identification based diagnostic scheme.

Consider a discrete LTI model that is described as follows:

$$\begin{aligned} x(k+1) &= Ax(n) + B(u(k) + f_a(k)) + w(k) \\ y(k) &= Cx(k) + D(u(k) + f_a(k)) + f_s(k) + v(k) \end{aligned} \tag{3}$$

where the input, state and output vectors are $u(k) \in \Re^l$, $x(k) \in \Re^n$ and $y(k) \in \Re^m$, respectively. Furthermore, $f_a(k) \in \Re^l$, $f_s(k) \in \Re^m$, $w(k) \in \Re^n$ and $v(k) \in \Re^m$ represent the actuator faults, sensor faults, actuator noise and sensor noise, respectively. The matrices A, B, C and D are constant matrices of appropriate dimensions.

Consider the system described in Equation (3) that is written in recursive form with s number of samples such that $s > n$ as follows:

$$\begin{aligned} y_s(k) &= \begin{bmatrix} y(k-s) & y(k-s+1) & \cdots & y(k) \end{bmatrix}^T \\ u_s(k) &= \begin{bmatrix} u(k-s) & u(k-s+1) & \cdots & u(k) \end{bmatrix}^T \end{aligned} \tag{4}$$

In a similar fashion, $f_s(k)$, $f_a(k)$, $w_s(k)$ and $v_s(k)$ could be constructed. The output of the system could be written as

$$\begin{aligned} y_s(k) &= \Psi x(k-s) + M_{us}u_s(k) + M_{us}f_{a,s}(k) \\ &\quad + N_{ds}w_s(k) + f_s(k) + v_s(k) \end{aligned} \tag{5}$$

where

$$M_{us} = \begin{bmatrix} 0 & 0 & \cdots & 0 \\ C & 0 & \cdots & 0 \\ \vdots & \vdots & \ddots & \vdots \\ CA^{s-1} & CA^{s-2} & \cdots & 0 \end{bmatrix}, N_{ds} = \begin{bmatrix} D & 0 & \cdots & 0 \\ CB & D & \cdots & 0 \\ \vdots & \vdots & \ddots & \vdots \\ CA^{s-1}B & CA^{s-2}B & \cdots & D \end{bmatrix} \tag{6}$$

$$\Psi = \begin{bmatrix} C & CA & \cdots & CA^s \end{bmatrix} \tag{7}$$

Let the residual be defined as

$$Y(k) = \begin{bmatrix} \hat{M} & -\hat{N} \end{bmatrix} \begin{bmatrix} y_s(k) \\ u_s(k) \end{bmatrix} = \begin{bmatrix} \Psi^\perp & -\Psi^\perp M_{us} \end{bmatrix} \begin{bmatrix} y_s(k) \\ u_s(k) \end{bmatrix} \tag{8}$$

$$Y(k) = \Psi^\perp y_s(k) - \Psi^\perp M_{us} u_s(k) \tag{9}$$

$\Psi^{\perp}$ is defined as the parity space of the system, such that $\Psi^{\perp}\Psi = 0$. Substituting Equation (5) into Equation (9),

$$Y(k) = \Psi^{\perp}(M_{us}f_{a,s}(k) + N_{ds}w_{s}(k) + f_{s}(k) + v_{s}(k)) \tag{10}$$

Equation (10) states that, if there is no fault in the system, the generated residual would only be having the effect of disturbance and noise acting on the actuators and sensors. According to Equations (8) and (9), due to the unavailability of the state-space model, our main objective for data-driven diagnostic system is to identify the left coprime factorization $(\Psi^{\perp}, \Psi^{\perp}M_{us})$ of the underlying system from healthy input–output data. N number of input–output data samples are collected during the healthy operation of the process. Assume that the order of the system is n, and indices p and f refer to the past and future, whereas $s = s_p = s_f$. From healthy input–output data, past and future input–output block Hankel matrices are constructed by subdividing data samples into past and future data samples, as

$$U_p = \begin{bmatrix} u_{s_p}(k) & u_{s_p}(k+1) & \cdots & u_{s_p}(k+N-1) \end{bmatrix} \in \Re^{s_p l \times N}$$
$$Y_p = \begin{bmatrix} y_{s_p}(k) & y_{s_p}(k+1) & \cdots & y_{s_p}(k+N-1) \end{bmatrix} \in \Re^{s_p m \times N}$$
$$U_f = \begin{bmatrix} u_{s_f}(k+s_p+1) & \cdots & u_{s_f}(k+s_f+N) \end{bmatrix} \in \Re^{s_f l \times N}$$
$$Y_f = \begin{bmatrix} y_{s_f}(k+s_p+1) & \cdots & y_{s_f}(k+s_f+N) \end{bmatrix} \in \Re^{s_f m \times N}$$

Here, u_{s_p}, u_{s_f}, y_{s_p} and y_{s_d} are represented as in Equation (4). For a fault free case, a future values data matrix could be written as

$$Z_p = \begin{bmatrix} Y_{s_p} \\ U_{s_p} \end{bmatrix}, \ Z_f = \begin{bmatrix} Y_{s_f} \\ U_{s_f} \end{bmatrix} \tag{11}$$

$$Z_f = \begin{bmatrix} \Psi & M_{us} \\ 0 & I \end{bmatrix}\begin{bmatrix} X_i \\ U_f \end{bmatrix} + \Theta, \ \Theta = \begin{bmatrix} N_{ds} & I \\ 0 & 0 \end{bmatrix}\begin{bmatrix} W_p \\ V_p \end{bmatrix} \tag{12}$$

for $N \gg s$, where $s \approx s_p \approx s_f > n$, and the covariance matrix of the collected data could be constructed as follows:

$$\frac{1}{N}Z_f Z_p = \frac{1}{N}\begin{bmatrix} \Psi & M_{us} \\ 0 & I \end{bmatrix}\begin{bmatrix} X_i \\ U_f \end{bmatrix}Z_p + \frac{1}{N}\Theta Z_p \tag{13}$$

and the matrix Z_p is also known as an instrumentation variable used to remove the effect of noise. It is assumed that the noise in the system is uncorrelated with the collected I/O data. Furthermore, to normalize data, Equation (13) is divided by N. A singular value decomposition of covariance matrix would lead to the identification of left coprime factors or data-driven residual as follows:

$$SVD(\frac{1}{N}Z_f Z_p) = U_z \begin{bmatrix} S_{z,1} & 0 \\ 0 & S_{z,2} \end{bmatrix}V_z^T, \ U_z = \begin{bmatrix} U_{z11} & U_{z12} \\ U_{z21} & U_{z22} \end{bmatrix}$$

Here,

$$S_{z_1} \in \Re^{ms_f \times (ms_f+n)} \qquad S_{z_s} \in \Re^{(ms_f-n) \times (ms_f+ls_p-ls_f-n)}$$
$$U_{z,11} \in \Re^{ms_f \times (ls_f+n)} \qquad U_{z,12} \in \Re^{ms_f \times (ms_f-n)} \tag{14}$$
$$U_{z,22} \in \Re^{ls_f \times (ms_f-n)}$$

and the parameter $\Psi^{\perp}$ and $\Psi^{\perp}M_{us}$ would be identified as [27]

$$\Psi^{\perp} = U_{z_{12}}^T \quad \Psi^{\perp}M_{us} = -U_{z_{22}}^T \tag{15}$$

By substituting the identified parameters in Equation (9), the residual can be constructed as given below:

$$Y(k) = \Psi^\perp (M_{us} f_{a,s}(k) + N_{ds} w_s(k) + f_s(k) + v_s(k))$$

The above equation indicates that, despite the fault-free case, the residual will be affected by noise and disturbances. It is of vital importance to obtain optimal parity space that also mitigates the effect of noise and disturbances in the residual. The procedure for identifying a subspace-based residual using I/O data is summarized in Algorithm 1.

Algorithm 1 SIM based fault detection algorithm

1: Collect the I/O data from plant during healthy operation
2: Estimate the order n of the system and set $s_f = s_p \approx s > n$
3: Construct block hankel matrices U_p, U_f, Y_p and Y_f
4: Construct the covariance matrix using Equation (13)
5: Obtain the $\Psi^\perp$ and $\Psi^\perp M_{us}$ using Equation (15)
6: Construct the residual as defined in Equation (9)

Proposed Robustness Method

The robustness problem could be modeled as selecting the parity vector from parity space to enhance the sensitivity towards faults and be less sensitive against noise and disturbances. The residual, defined in Equation (9), contains the matrices M_{us} and N_{ds} also known as fault and disturbance coupling matrix, respectively. Choosing parity vector $\Psi^\perp$, which solves the objective function defined in Equation (16), maximizes the M_{us} and minimizes the N_{ds}, which could lead to the insensitivity towards sensor fault and noise:

$$J_1 = \max_{\Psi_s^\perp} \frac{\Psi_s^\perp M_{us} M_{us}^T \Psi_s^{\perp T}}{\Psi_s^\perp N_{ds} N_{ds}^T \Psi_s^{\perp T}} \tag{16}$$

To increase sensitivity towards a sensor fault, index J_2 was proposed in [37] defined in Equation (17)

$$J_2 = \max_{\Psi_s^\perp} \frac{\Psi_s^\perp N_{ds} N_{ds}^T \Psi_s^{\perp T}}{\Psi_s^\perp M_{us} M_{us}^T \Psi_s^{\perp T}} \tag{17}$$

Index (17) solves the problem for sensitivity towards sensor faults but performs worst in case of an actuator fault because the actuator fault coupling matrix is maximized. To solve this issue, a performance index is proposed as follows:

$$Y(k) = \Psi_s^\perp (Y_s(k) - M_{us} U_s(k))$$
$$Y(k) = \Psi_s^\perp (M_{us} f_a(k) + N_{ds} w_s(k) + f_s(k) + v_s(k))$$
$$Y(k) = \Psi_s^\perp \left([M_{us}\ I][F_a(k)\ F_s(k)]^T + [N_{ds}\ I][W_s(k)\ V_s(k)]^T \right)$$
$$Y(k) = \Psi_s^\perp (M_{usi}\ F(k) + N_{dsi}\ D(k))$$

Now, the combined effect of fault and disturbance could be defined in the following way:

$$R_{wv} = \|\ N_{dsi}(S)\ \|_\infty \quad S_{as} = \|\ M_{usi}(S)\ \|_\infty \tag{18}$$

where S is design parameter, in this case, parity vector. Now, the performance index could be defined as

$$J_3 = \max_{\Psi_s^\perp} \frac{S_{as}}{R_{wv}} \Rightarrow \max_{\Psi_s^\perp} \frac{\Psi_s^\perp M_{usi} M_{usi}^T \Psi_s^{\perp T}}{\Psi_s^\perp N_{dsi} N_{dsi}^T \Psi_s^{\perp T}} \tag{19}$$

To solve index J_3, a generalized eigenvalue problem could be used as follows:

$$l_s(\Psi_s^\perp N_{dsi} N_{dsi}^T \Psi_s^{\perp T} - \lambda_s \Psi_s^\perp M_{usi} M_{usi}^T \Psi_s^{\perp T}) = 0 \tag{20}$$

l_s is the eigenvector that maximizes the M_{usi} and minimizes the N_{dsi}, where λ_s is the corresponding eigenvalue. The procedure for robust residual construction could be summarized as follows in Algorithm 2.

Algorithm 2 SIM based robust fault detection algorithm

1: Using Algorithm 1 obtain the parameter $\Psi_s^\perp$ and $\Psi_s^\perp M_u s$
2: Solve (20) to obtain eigenvector l_s
3: Obtain the robust residual generator as follows

$$\Psi_{s,rob}^\perp = l_s \Psi_s^\perp$$

4: Construct the residual as

$$Y_{rob}(k) = \Psi_{s,rob}^\perp y_s(k) - \Psi_{s,rob}^\perp M_{us} u_s(k) \tag{21}$$

---

4. Robust Fault Isolation Method

Fault isolation deals with identifying faulty components and hence plays an important role in FDI. Our modified robust isolation algorithm is based on decoupling the effect of all faults from the desired residual. For example, the jth residual $Y_j(k)$ would be decoupled from all other faults $f_1(k), \ldots, f_{j-1}, f_{j+1}, \ldots, f_{k_f}(k)$ and sensitive towards f_j, where k_f represents the total number of faults. Hence, a bank of residuals would be needed to isolate a single fault from others. Further information about isolated faults would be extracted from the combination of multiple residuals, assuming that only a single fault would occur at any instant. If the process under consideration has m sensors and k_f number of faults where $m < k_f$ and one fault is required to be isolated from the remaining faults, the perfect isolation could be used by constructing ${}^{k_f}C_{m-1}$, and each residual would be a function of different faults. As shown, the final result about the fault in a specific component for the induction motor could be constructed using Table 3. The procedure for residual generation for Sensor fault isolation could be summarized in Algorithm 3 and procedure for residual generation for Actuator fault isolation could be summarized in Algorithm 4.

Table 3. Fault isolation logic.

	Y_1	Y_2	Y_3	Y_4
f_1	1	0	1	1
f_2	0	1	1	1
f_3	1	1	1	0
f_4	1	1	0	1

Algorithm 3 Sensor Fault Isolation

1: Obtain the matrices $\Psi_s^\perp$ and $\Psi_s^\perp M_{us}$ using Algorithm 1
2: Divide $\Psi_s^\perp$ in the following way: $\Psi_s^\perp = [\Psi_{s,1}^\perp \; \Psi_{s,2}^\perp \; \dots \; \Psi_{s,s_g}^\perp]$, where $\Psi_{s,j}^\perp \in \Re^{\mu \times m}$ and $j = 1, 2, \dots, s_g$
3: Further sub-divide the $\Psi_{s,j}^\perp = [\Psi_{s,j,1}^\perp \; \Psi_{s,j,2}^\perp \; \dots \; \Psi_{s,j,m}^\perp]$ such that $\Psi_{s,j,k}^\perp \in \Re^\mu$, $k = 1, 2, \dots, m$. m represents the number of outputs
4: Now parity space for all other faults, except i_{th} fault, could be written as: $\Psi_{s,i}^\perp = [\Psi_{s,1,1}^\perp \dots \Psi_{s,1,i-1}^\perp \; \Psi_{s,1,i+1}^\perp \dots \Psi_{s,1,m}^\perp \Psi_{s,2,1}^\perp \dots \; \Psi_{s,2,i-1}^\perp \Psi_{s,2,i+1}^\perp \dots \Psi_{s,2,m}^\perp \dots \Psi_{s,s_g,i-1}^\perp \; \Psi_{s,s_g,i+1}^\perp \dots \Psi_{s,s_g,m}^\perp]$
5: Find the null space for all sensors except i^{th} sensor as $L_{sen,i}\Psi_{s,i}^\perp = 0$ and now the parity space for i^{th} sensor would be $\Psi_{s,sen,i}^\perp = L_{sen,i}\Psi_s^\perp$
6: Find the robust parity vector from identified parity space for i^{th} sensor as

$$J_{3,sen} = \max_{\Psi_{s,sen,i}^\perp} \frac{\Psi_{s,sen,i}^\perp M_{usi} M_{usi}^T \Psi_{s,sen,i}^{\perp T}}{\Psi_{s,sen,i}^\perp N_{dsi} H_{dsi}^T \Psi_{s,sen,i}^{\perp T}} \qquad (22)$$

7: To solve index (19), a generalized eigenvalue problem can be used as

$$l_{s,sen,i}(\Psi_{s,sen,i}^\perp H_{usi} H_{usi}^T \Psi_{s,sen,i}^{\perp T} - \lambda_{s,sen,i} H_{dsi} H_{dsi}^T \Psi_{s,sen,i}^{\perp T}) = 0$$

8: Construct the residual generator as for i^{th} sensor as

$$\Upsilon_{sen,i} = l_{s,sen,i}(\Psi_{s,sen,i}^\perp y_s(k) - \Psi_{s,sen,i}^\perp M_{us} u_s(k)) \qquad (23)$$

Algorithm 4 Actuator fault Isolation

1: Set $\xi_s = \Psi_s^\perp M_{us}$
2: Divide ξ_s in the following way: $\xi_s = [\xi_{s,1} \; \xi_{s,2} \; \dots \; \xi_{s,s_g}]$, where $\xi_{s,j} \in \Re^{\mu \times l}$ and $j = 1, 2, \dots, s_g$
3: Further sub-divide the $\xi_{s,j} = [\xi_{s,j,1} \; \xi_{s,j,2} \; \dots \; \xi_{s,j,m}]$ such that $\xi_{s,j,k} \in \Re^\mu$, $k = 1, 2, \dots, m$, where m represents the number of outputs
4: Now, parity space for all other faults, except ith fault, could be written as $\xi_{s,i} = [\xi_{s,1,1} \dots \xi_{s,1,i-1} \; \xi_{s,1,i+1} \dots \xi_{s,1,m} \xi_{s,2,1} \dots \; \xi_{s,2,i-1}$

$$\xi_{s,2,i+1} \dots \xi_{s,2,m} \dots \xi_{s,s_g,i-1} \; \xi_{s,s_g,i+1} \dots \xi_{s,s_g,m}]$$

5: Find the null space for all actuators except i^{th} actuator as $P_{act,i}\xi_{s,i} = 0$ and now the parity space for i^{th} actuator would be $\Psi_{s,act,i} = P_{sen,i}\Psi_s$
6: Find the robust parity vector from identified parity space for i^{th} actuator as

$$J_{3,act} = \max_{\Psi_{s,act,i}} \frac{\Psi_{s,act,i} M_{usi} M_{usi}^T \Psi_{s,act,i}^T}{\Psi_{s,act,i} N_{dsi} N_{dsi}^T \Psi_{s,act,i}^T} \qquad (24)$$

7: To solve index (19), generalized eigenvalue problem can be used as $l_{s,act,i}(\Psi_{s,act,i} M_{usi} M_{usi}^T \Psi_{s,act,i}^T - \lambda_{s,act,i} N_{dsi} N_{dsi}^T \Psi_{s,act,i}^T) = 0$
8: Construct the residual generator as for i^{th} sensor as

$$\Upsilon_{act,i} = l_{s,act,i}(\Psi_{s,act,i} y_s(k) - \Psi_{s,act,i} M_{us} u_s(k)) \qquad (25)$$

---

5. Residual Post-Processing

5.1. Residual Evaluation Method

For the evaluation of residual, a threshold needs to be computed empirically (fixed) or statistically. In order to quantify the error rate, a stochastic threshold must be computed to make an accurate decision about whether a fault has occurred. Reduction of false negative alarms depends upon the noise level present in the sensor measurements and sensitivity to faults. Assuming the noise present in the system is distributed normally, we are using the Gaussian Likelihood Ratio (GLR) test for designing a threshold and evaluating residual. The procedure for applying GLR-based threshold is described in Algorithm 5.

Algorithm 5 GLR Test

1: Choose a confidence interval and select value of χ_a using Chi-square table such the $prob(\chi_a < \chi) = \alpha$

2: Obtain the threshold from $J_{th} = \frac{\chi_a}{2}$

3: Using residual signal, construct the statistical signal as $J = \frac{1}{2\sigma^2 N_w}\left(\sum_{i=1}^{N_w} Y(i)^2\right)$

4: If $J < J_{th}$ results are negative and there is not a fault; otherwise, a fault is detected for $J > J_{th}$.

5.2. Wavelet Transformation of Residual

Fourier analysis of residual is based on dividing the signal into its sine and cosine components by transforming from a time to frequency domain. However, wavelet transform is different from Fourier in the sense that it uses functions that are localized in Fourier and real space as well. It decomposes the signal into approximate and detailed coefficients. As the residual signal is affected by noise, the detailed coefficients are discarded due to the large impact of disturbances on them. Wavelet transform is generally represented by the following function:

$$G(a,b) = \int_{-\infty}^{\infty} Y(t)\psi^*(\frac{t-b}{a})dt \tag{26}$$

which continues in the range of a and b and adds more computational complexity. Since we are dealing with discrete time signals, discrete wavelet transform could be used. This discrete transform would decompose the signal into wavelets that are mutually orthogonal to each other:

$$Y(t) = w_0 + \sum_{j=0}^{\infty}\sum_{k=0}^{2j-1} w_{2j+k}\psi(2^j t - kT) \tag{27}$$

where

$$w_0 = \int_0^T Y(t)dt$$

$$w_{2j+k} = \int_0^T Y(t)\psi(2^j t - kT)dt$$

6. Online Implementation and Results

The induction motor (SE2672-3G) as shown in Figure 1 is started in $Y-$configuration and loaded with its nominal torque, and the motor runs at its nominal speed.

Now, 1200 samples are collected with sampling time of $T_s = 0.1$ s. With $s_f = 8$, $n = 4$, the identified parity space $\Psi^\perp \in \Re^{12\times16}$ and $\Psi^\perp M_{us} \in \Re^{12\times16}$. Now, based on Equation (21), three different residuals are constructed using index (16), (17) and (19). The generated residuals are shown in Figure 3.

Various types of faults could occur during the operational state of the induction motor, including insulation breaking of the stator field winding, excessive current increase due to overloading, measurement devices such as ampere/volt meter could become defective, and supply voltage (modeled as an actuator) could become defective in the case of an

unreliable power source. The profile of fault could be step, ramp, sinusoidal, etc., based on the conditions and nature of faulty components in the motor.
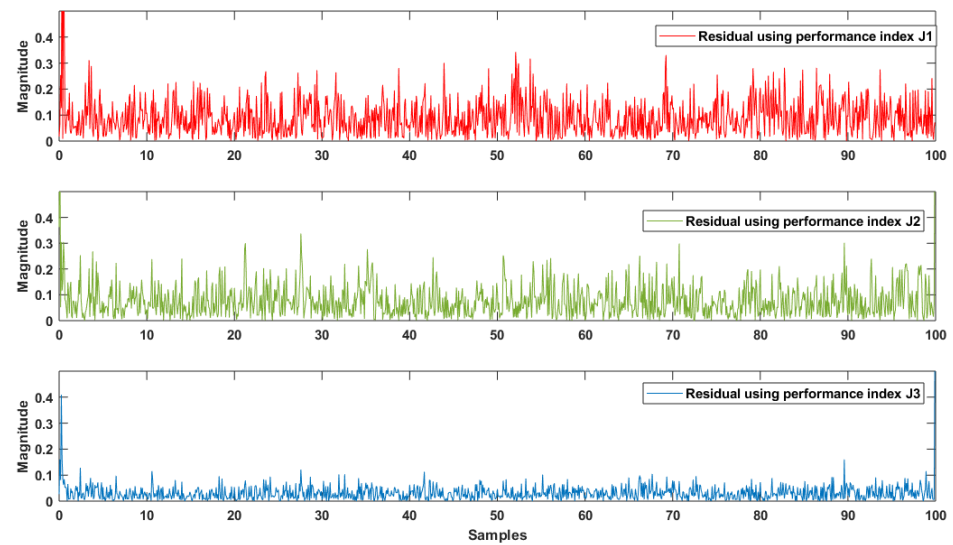

Figure 3. Residual with no faults.

The computed variance for generated residuals is $\text{var}(Y_{J_1}) = 0.0133$, $\text{var}(Y_{J_2}) = 0.0103$ and $\text{var}(Y_{J_3}) = 0.0075$, which shows the reduction of noise power in residual computed through the proposed index in the absence of a fault.

Consider the representation of faults as

$$
\begin{aligned}
f_1 &\rightarrow fault\ in\ stator\ voltages\ q-axis\ (v_q)\\
f_2 &\rightarrow fault\ in\ stator\ voltages\ d-axis\ (v_d)\\
f_3 &\rightarrow fault\ in\ stator\ current\ q-axis\ (i_q)\\
f_4 &\rightarrow fault\ in\ stator\ current\ d-axis\ (i_d)
\end{aligned}
$$

A pulse fault is introduced in the actuator 1 (17–25 s) and sensor 2 (83–92 s), and the resultant residual using J_1, J_2 and J_3 is shown in Figure 4.
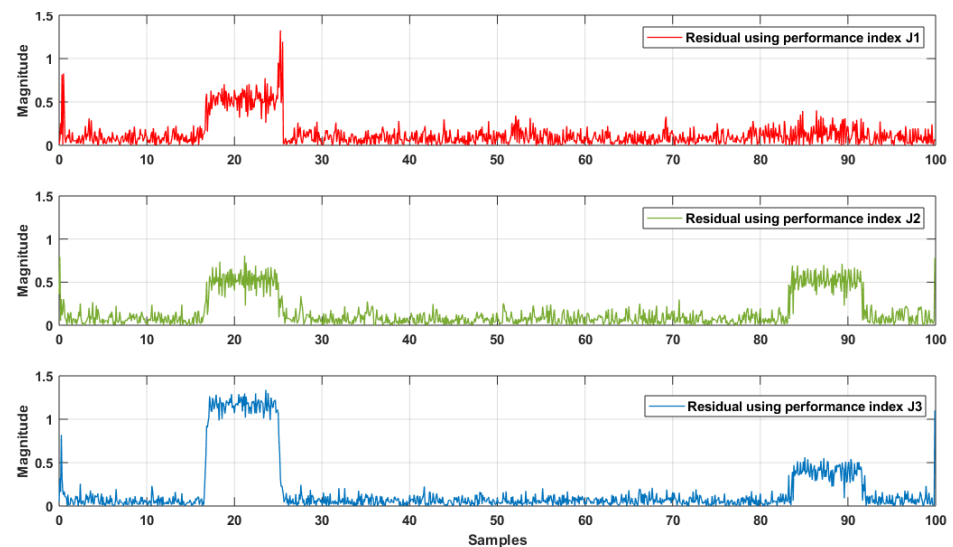

Figure 4. Residual with stator current (i_q) and stator voltage (v_d) faults.

Performance of the residual generator is also estimated by measuring the standard deviation and variance of generated residuals. Statistical data for residuals obtained using performance index J_1, J_2 and J_3 are shown in Table 4.

Table 4. Statistics for indices J_1, J_2 and J_3.

	$\mathbf{Y}_{J_1}$	$\mathbf{Y}_{J_2}$	$\mathbf{Y}_{J_3}$
variance	0.0242	0.0327	0.0992
standard deviation	0.1556	0.1809	0.3151

From Table 4 it is clear the J_2 performs better than J_1 due to more variance and detectability. Similarly, statistical data for J_3 are shown in Table 4 and also show that the standard deviation and variance of generated residual are greater than J_1 and J_2, which is also the reason for better detectability of faults. The false alarm rate (FAR) and false detection rate (FDR) for performance index J_1, J_2 and J_3 are shown in Table 5.

Table 5. FAR and FDR for indices J_1, J_2 and J_3.

	J_1	J_2	J_3
FAR	4.27	1.63	0.85
FDR	82.53	97.61	98.88

Fault Isolation

In three phase induction motor (SG-2672), there are two sensors and two actuator faults. The current in the $d - q$ axis is modeled as sensors 1 and 2, respectively, while the applied AC power supply for the $d - q$ axis is modeled as actuators 1 and 2, respectively. Applying Algorithms 1 and 2 would indicate the presence of the fault in the motor, but it would not specify the location of the faulty component. For that purpose, we would use a modified isolation procedure in Algorithms 3 and 4 based on perfect unknown input decoupling.

Parity spaces, $\Psi^{\perp}$ and $\Psi^{\perp} M_{us}$, obtained using Algorithms 1 and 2, are being used for actuator and sensor fault isolation using proposed robust parity vectors $l_{s,act,i}$ and $l_{s,sen,i}$, respectively.

Since m = 2 and $k_f = 4$, a total of four residuals Y_1, Y_2, Y_3, Y_4 are generated based on $^4C_2$.

Furthermore, representing the residual as a function of faults as in Equation (28),

$$\begin{aligned}
Y_1(k) &= F(f_1, f_3, f_4) \\
Y_2(k) &= F(f_2, f_3, f_4) \\
Y_3(k) &= F(f_1, f_2, f_3) \\
Y_4(k) &= F(f_1, f_2, f_4)
\end{aligned} \tag{28}$$

A fault is introduced in the d-q axis of stator voltages (actuator 1, 2) and d-axis stator current for different time intervals, The faults are then detected online using Algorithm 2, and residual is evaluated based on the GLR threshold as shown in Figure 5. Furthermore, using Algorithm 3 and 4, residuals are constructed for indication of faulty components as shown in Figure 6. Now, at any instant, a decision about faults in specific components could be made using Table 3. It is evident from the figure that faults have occurred in stator voltages (v_q, v_d) and current (i_q) during specified time intervals.

Generally, the nature of the faults is of low frequency so applying wavelet transform and keeping only approximate coefficients (containing lower frequencies of the residual) could reduce the false alarm rate as shown in Figure 7.
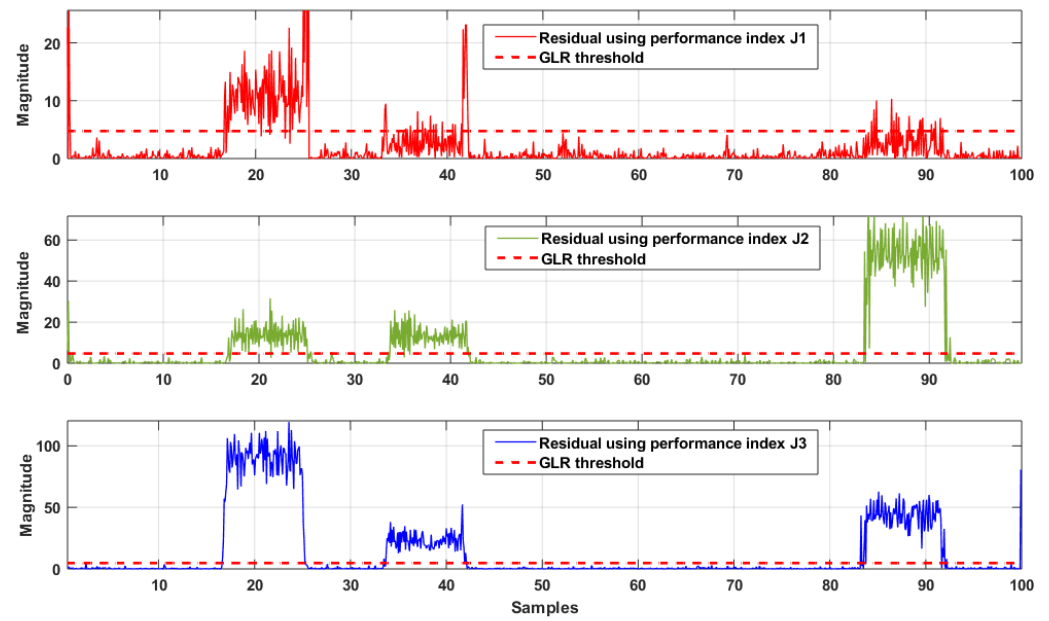
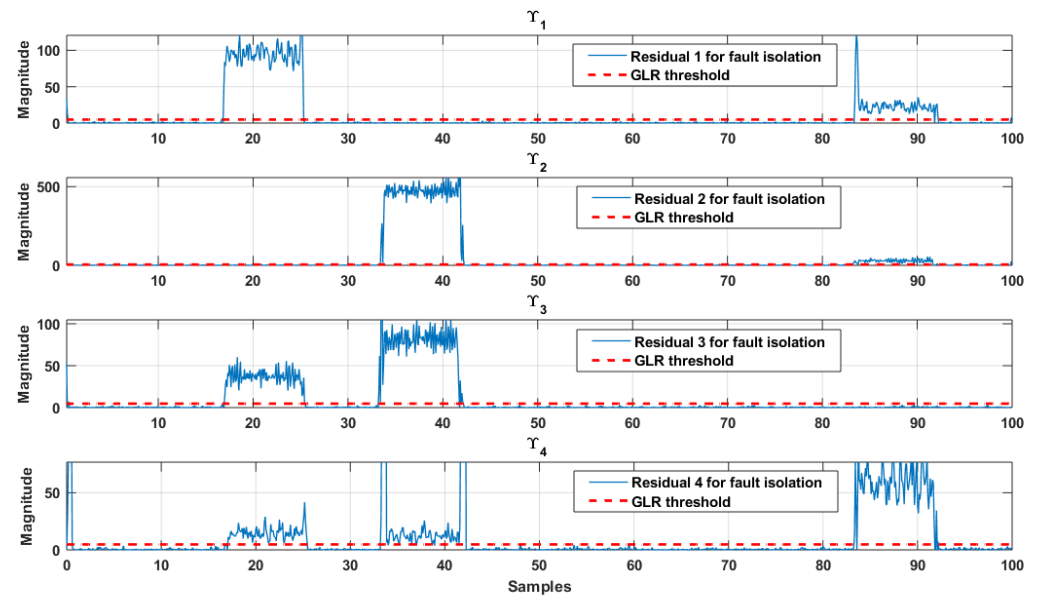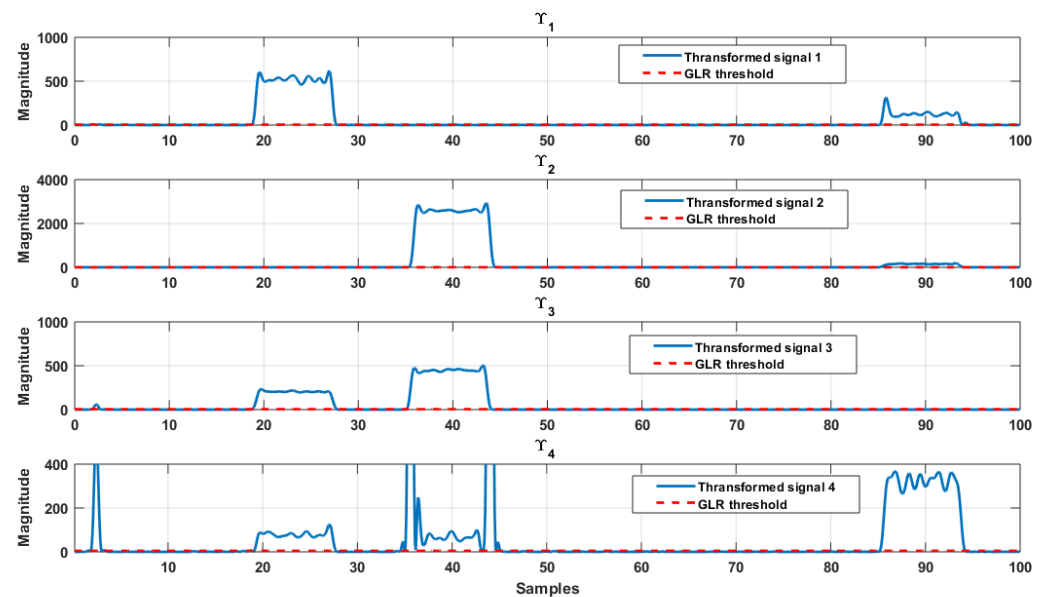**Figure 5.** Residual with stator voltages (v_q, v_d) and current (i_d) faults.

Figure 6. Fault isolation for stator voltages (v_q, v_d) and current (i_d) faults.

Figure 7. Fault isolation for stator voltages (v_q, v_d) and current (i_q) faults with wavelet transformation.

7. Conclusions

In this paper, we have presented a robust data-driven fault detection and isolation scheme for the systems with unknown dynamics. The proposed scheme showed robustness against sensor noise and actuator disturbances. The existing parity vector identification methodology is modified with the proposed performance index for a simultaneous increase in sensitivity towards faults and robustness against disturbances. Generated robust parity space is further used for the residual generation, which is further post-processed by wavelet transformation. Compared with previously defined performance indexes, our scheme with the proposed performance index has shown better statistics of reduced false alarm rate and increased false detection rate. An unknown input decoupling-based fault isolation procedure is adopted to designate the fault location. This procedure is also modified with our performance index to enhance sensitivity towards faults and considerably reduce the effect of noise on residuals compared to previously proposed indexes. Wavelet transform is used to discard the high-frequency content of the residual to further enhance FDR. The robust data-driven fault detection and isolation scheme is applied to the experimental setup of an induction motor in the lab. Obtained results showed the efficacy of the proposed fault diagnosis system.

8. Limitations

The proposed methodology is proved to be more effective, especially for linear dynamic systems. The less online computation and reduced false alarm rate are the added benefits of the designed scheme. Meanwhile, it is observed that the proposed strategy has limited efficacy for the highly nonlinear dynamic system as it uses a linear dynamic approach for subspace identification. In addition, for modern large-scale industrial processes, having many sensors makes the task of health monitoring very complex and expensive simultaneously. It demands key performance indicators based on fault diagnosis for alarm management to eradicate redundant alarms.

9. Future Work

Our work on a robust data-driven method can be further used for fault identification and fault tolerant control systems as these are also vital to guarantee the process's sub-optimal function in the fault's existence.

References

1. Isermann, R. *Fault-Diagnosis Systems: An Introduction from Fault Detection to Fault Tolerance*; Springer Science & Business Media: Berlin/Heidelberg, Germany, 2006.
2. Blanke, M.; Kinnaert, M.; Lunze, J.; Staroswiecki, M.; Schröder, J. *Diagnosis and Fault-Tolerant Control*; Springer: Berlin/Heidelberg, Germany, 2006; Volume 2.
3. Ding, S.X. *Model-Based Fault Diagnosis Techniques: Design Schemes, Algorithms, and Tools*; Springer Science & Business Media: Berlin/Heidelberg, Germany, 2008.
4. Gertler, J. *Fault Detection and Diagnosis in Engineering Systems*; Routledge: London, UK, 2017.
5. Abbasi, M.A.; Khan, A.Q.; Abid, M.; Mustafa, G.; Mehmood, A.; Luo, H.; Yin, S. Parity-based robust data-driven fault detection for nonlinear systems using just-in-time learning approach. *Trans. Inst. Meas. Control* **2020**, *42*, 1690–1699. [CrossRef]
6. Khan, A.S.; Khan, A.Q.; Iqbal, N.; Mustafa, G.; Abbasi, M.A.; Mahmood, A. Design of a computationally efficient observer-based distributed fault detection and isolation scheme in second-order networked control systems. *ISA Trans.* **2022**, *128*, 229–241. [CrossRef]
7. Ahmad, M.; Mohd-Mokhtar, R. A Survey on Model-based Fault Detection Techniques for Linear Time-Invariant Systems with Numerical Analysis. *Pertanika J. Sci. Technol.* **2022**, *30*, 53–78. [CrossRef]
8. Song, J.; He, X. Model-based fault diagnosis of networked systems: A survey. *Asian J. Control.* **2021**, *24*, 526–536. [CrossRef]
9. Bernardi, E. Fault-tolerant Model-based Predictive Control Applied to Industrial Processes. Ph.D. Thesis, Universidad Autónoma de Yucatán Sábado, Mérida, Mexico, 2021.
10. Naderi, E.; Khorasani, K. A data-driven approach to actuator and sensor fault detection, isolation and estimation in discrete-time linear systems. *Automatica* **2017**, *85*, 165–178. [CrossRef]
11. Paya, B.; Esat, I.; Badi, M. Artificial neural network based fault diagnostics of rotating machinery using wavelet transforms as a preprocessor. *Mech. Syst. Signal Process.* **1997**, *11*, 751–765. [CrossRef]
12. Ma, S.; Cai, W.; Liu, W.; Shang, Z.; Liu, G. A lighted deep convolutional neural network based fault diagnosis of rotating machinery. *Sensors* **2019**, *19*, 2381. [CrossRef] [PubMed]
13. Wilhelm, Y.; Reimann, P.; Gauchel, W.; Mitschang, B. Overview on hybrid approaches to fault detection and diagnosis: Combining data-driven, physics-based and knowledge-based models. *Procedia CIRP* **2021**, *99*, 278–283. [CrossRef]
14. Li, Z.; Gao, Y.; Zhang, X.; Wang, B.; Ma, H. A Model-Data-Hybrid-Driven Diagnosis Method for Open-Switch Faults in Power Converters. *IEEE Trans. Power Electron.* **2021**, *36*, 4965–4970. [CrossRef]
15. Abbasi, M.A.; Khan, A.Q.; Mustafa, G.; Abid, M.; Khan, A.S.; Ullah, N. Data-driven fault diagnostics for industrial processes: An application to Penicillin fermentation process. *IEEE Access* **2021**, *9*, 65977–65987. [CrossRef]
16. Argawal, R.; Kalel, D.; Harshit, M.; Domnic, A.D.; Singh, R.R. Sensor Fault Detection using Machine Learning Technique for Automobile Drive Applications. In Proceedings of the 2021 National Power Electronics Conference (NPEC), Bhubaneswar, India, 15–17 December 2021; pp. 1–6.
17. Liu, X.; Zhou, Q.; Zhao, J.; Shen, H.; Xiong, X. Fault diagnosis of rotating machinery under noisy environment conditions based on a 1-D convolutional autoencoder and 1-D convolutional neural network. *Sensors* **2019**, *19*, 972. [CrossRef] [PubMed]
18. Wang, Y.; Zheng, D.; Jia, R. Fault Diagnosis Method for MMC-HVDC Based on Bi-GRU Neural Network. *Energies* **2022**, *15*, 994. [CrossRef]
19. Yin, Shen Data-Driven Design of Fault Diagnosis Systems. Ph.D. Thesis, Universität Duisburg-Essen, Duisburg, Germany, 2012.
20. Daemi, A.; Gopaluni, B.; Huang, B. Process Monitoring using Domain-Adversarial Probabilistic Principal Component Analysis: A Transfer Learning Framework. *IEEE Trans. Ind. Inform.* **2022**, *Early Access*. [CrossRef]
21. Nguyen, V.H.; Golinval, J.C. Fault detection based on kernel principal component analysis. *Eng. Struct.* **2010**, *32*, 3683–3691. [CrossRef]
22. Lee, G.; Han, C.; Yoon, E.S. Multiple-fault diagnosis of the Tennessee Eastman process based on system decomposition and dynamic PLS. *Ind. Eng. Chem. Res.* **2004**, *43*, 8037–8048. [CrossRef]

23. Muradore, R.; Fiorini, P. A PLS-based statistical approach for fault detection and isolation of robotic manipulators. *IEEE Trans. Ind. Electron.* **2011**, *59*, 3167–3175. [CrossRef]

24. Zhang, Y.; Teng, Y.; Zhang, Y. Complex process quality prediction using modified kernel partial least squares. *Chem. Eng. Sci.* **2010**, *65*, 2153–2158. [CrossRef]

25. Dong, J. Data Driven Fault Tolerant Control: A Subspace Approach. Ph.D. Thesis, Delft University of Technology, Delft, The Netherlands, 2009.

26. Ding, S.; Zhang, P.; Naik, A.; Ding, E.; Huang, B. Subspace method aided data-driven design of fault detection and isolation systems. *J. Process Control* **2009**, *19*, 1496–1510. [CrossRef]

27. Wang, Y.; Ma, G.; Ding, S.X.; Li, C. Subspace aided data-driven design of robust fault detection and isolation systems. *Automatica* **2011**, *47*, 2474–2480. [CrossRef]

28. Peng, K.; Wang, M.; Dong, J. Event-triggered fault detection framework based on subspace identification method for the networked control systems. *Neurocomputing* **2017**, *239*, 257–267. [CrossRef]

29. Van Overschee, P.; De Moor, B. *Subspace Identification for Linear Systems: Theory-Implementation-Applications*; Springer Science & Business Media: Berlin/Heidelberg, Germany, 2012.

30. Ding, S.X. *Data-Driven Design of Fault Diagnosis and Fault-Tolerant Control Systems*; Springer: Berlin/Heidelberg, Germany, 2014.

31. Yin, S.; Ding, S.X.; Haghani, A.; Hao, H.; Zhang, P. A comparison study of basic data-driven fault diagnosis and process monitoring methods on the benchmark Tennessee Eastman process. *J. Process Control* **2012**, *22*, 1567–1581. [CrossRef]

32. Hussain, A.; Khan, A.Q.; Abid, M. Robust fault detection using subspace aided data driven design. *Asian J. Control* **2016**, *18*, 709–720. [CrossRef]

33. Yin, S.; Li, X.; Gao, H.; Kaynak, O. Data-based techniques focused on modern industry: An overview. *IEEE Trans. Ind. Electron.* **2014**, *62*, 657–667. [CrossRef]

34. Wei, X.; Verhaegen, M.; van Engelen, T. Sensor fault detection and isolation for wind turbines based on subspace identification and Kalman filter techniques. *Int. J. Adapt. Control Signal Process.* **2010**, *24*, 687–707. [CrossRef]

35. Dong, J.; Verhaegen, M. Data driven fault detection and isolation of a wind turbine benchmark. *IFAC Proc. Vol.* **2011**, *44*, 7086–7091. [CrossRef]

36. Kumar, R.; Cirrincione, G.; Cirrincione, M.; Tortella, A.; Andriollo, M. Induction Machine Fault Diagnosis Using Stator Current Subspace Spectral Estimation. In Proceedings of the 2018 21st International Conference on Electrical Machines and Systems (ICEMS), Jeju, Korea, 7–10 October 2018; pp. 2565–2570.

37. Tariq, M.F.; Khan, A.Q.; Abid, M.; Mustafa, G. Data-Driven Robust Fault Detection and Isolation of Three-Phase Induction Motor. *IEEE Trans. Ind. Electron.* **2018**, *66*, 4707–4715. [CrossRef]

38. Crowder, R. 7—Induction motors. In *Electric Drives and Electromechanical Systems*, 2nd ed.; Crowder, R., Ed.; Butterworth-Heinemann: Oxford, UK, 2020; pp. 187–207. [CrossRef]

39. Hutasuhut, A.A.; Pasaribu, F.I. *Design of Motor Induction 3-Phase from Waste Industry to Generator for Microhydro at Isolated Village*; IOP Conference Series; Materials Science and Engineering; IOP Publishing: Bristol, UK, 2017; Volume 237, p. 012021.

40. Kakosimos, P.E.; Sarigiannidis, A.G.; Beniakar, M.E.; Kladas, A.G.; Gerada, C. Induction motors versus permanent-magnet actuators for aerospace applications. *IEEE Trans. Ind. Electron.* **2013**, *61*, 4315–4325. [CrossRef]

41. Siddique, A.; Yadava, G.; Singh, B. A review of stator fault monitoring techniques of induction motors. *IEEE Trans. Energy Convers.* **2005**, *20*, 106–114. [CrossRef]

42. Siddiqui, K.M.; Sahay, K.; Giri, V. Health monitoring and fault diagnosis in induction motor-a review. *Int. J. Adv. Res. Electr. Electron. Instrum. Eng.* **2014**, *3*, 6549–6565.

43. Skowron, M.; Orlowska-Kowalska, T.; Wolkiewicz, M.; Kowalski, C.T. Convolutional neural network-based stator current data-driven incipient stator fault diagnosis of inverter-fed induction motor. *Energies* **2020**, *13*, 1475. [CrossRef]

44. Dai, X.; Gao, Z. From model, signal to knowledge: A data-driven perspective of fault detection and diagnosis. *IEEE Trans. Ind. Inform.* **2013**, *9*, 2226–2238. [CrossRef]

45. Gandhi, A.; Corrigan, T.; Parsa, L. Recent advances in modeling and online detection of stator interturn faults in electrical motors. *IEEE Trans. Ind. Electron.* **2010**, *58*, 1564–1575. [CrossRef]

46. Rodriguez-Blanco, M.A.; Golikov, V.; Vazquez-Avila, J.L.; Samovarov, O.; Sanchez-Lara, R.; Osorio-Sánchez, R.; Pérez-Ramírez, A. Comprehensive and Simplified Fault Diagnosis for Three-Phase Induction Motor Using Parity Equation Approach in Stator Current Reference Frame. *Machines* **2022**, *10*, 379. [CrossRef]

47. Sheikh, M.A.; Bakhsh, S.T.; Irfan, M.; Nor, N.b.M.; Nowakowski, G. A Review to Diagnose Faults Related to Three-Phase Industrial Induction Motors. *J. Fail. Anal. Prev.* **2022**, *22*, 1546–1557. [CrossRef]